

# Three Dimensional Analysis of Induced Detonation of Cased Explosive

Devon Downes<sup>1</sup>, Amal Bouamoul<sup>2</sup> and Manouchehr Nejad Ensan<sup>1</sup>

<sup>1</sup>*Aerospace Portfolio, National Research Council, Ottawa, ON, Canada*

<sup>2</sup>*Defence Research & Development Canada–Valcartier, Quebec City, QC, Canada*

## Abstract

*Fragments of aluminum impacting on Composition B explosive encased in rolled homogenous armour (RHA) steel were investigated through the LS-DYNA<sup>®</sup>. The investigation focused on shock to detonation simulations of Composition B, with the objective of determining both the critical velocity which would generate a shockwave strong enough to cause detonation of the explosive, as well as the resulting pressure profile of the detonation wave.*

*Detonation scenarios at low, intermediate and high impact velocities were investigated. It was observed that at low impact velocity the explosive failed to detonate. At intermediate velocities, detonation was due to the development of localized hot spots caused by the compression of the explosive from the initial shockwave. Detonation was also caused by pressure waves reflecting against the casing of the explosive leading to the so-called sympathetic detonation. At high impact velocity, initiation of the explosive was caused by the initial incident pressure wave located immediately behind the top casing/explosive interface.*

## 1. Introduction

A detailed understanding of the initiation of high explosives by shock waves generated from fragment impact is of great interest for defense, security and safety applications. Solutions that capture the essential features of this phenomenon are a challenging task that requires among others, shock pressures, critical velocity and the release of chemical energy in the explosive. The foundation for the critical velocity was based on an approach defined by Gurney [1] who derived analytical equations for a sphere and an indefinitely long cylinder. In general, the impact shock induced detonation behavior of an explosive is influenced significantly by the presence of a confinement of the explosive, i.e., the presence of the container walls. It has been reported that the explosive in a steel container showed a diminished threshold level of impact for detonation with more violent reaction sustained for an extended period of time when compared with an unconfined explosive [2]. The role of the explosive confinement on the detonation behavior varies depending on the position of the confinement wall relative to the impact location, whether the confinement is in the form of front plate (impacting plate), back plate (confinement wall on the opposite side of the impact plate), or lateral wall. In general, the presence of a cover plate in front of an explosive diminishes the detonation sensitivity of the explosive, as has been known from the early period of explosive sensitivity tests [3]. In the well-known empirical formula, the Jacobs–Roslund equation [4], the velocity threshold is modeled to be linearly proportional to the thickness of the cover plate material. Lawrence et al [5] modeled fragments impacting munitions

casing to determine the critical velocity required to initiate the explosive. They showed that for small diameter fragments the simulated critical velocity correlated well with the analytical velocity. However for large diameter fragments greater (>5mm), higher critical velocities than the Jacobs-Roslund are required.

In this paper a finite element analysis is performed to model the dynamic response of a steel box filled with a Comp B explosive caused by high velocity projectile impact, using the LS-DYNA [6]. The primary goal is to determine the threshold condition that causes detonation of the encased energetic material. A hemispherical shape projectile is considered. The threshold detonation velocity (critical velocity), the resulting shockwaves propagation and the pressure profile are presented.

## 2. Numerical Simulation

Although different numerical approaches for analysis of shock to detonation impact events are available, finite element analyses, which are based on accurate constitutive models, provide the most detailed information on the spatial and temporal distribution of impact events. The objective of the present research was to simulate the transient dynamic impact resulting from a collision between a fragments and casing, using the finite element analysis software LS-DYNA. This software is an explicit, nonlinear finite element code widely used by the defence and military to simulate structural failure, air/ water/ soil and container explosion. Features of this code include large material and element libraries, many contact algorithms and a high level of accuracy.

### 2.1 Finite Element Model Geometry

The finite element model developed is shown in Figure 1. This model contained four major parts: fragment, explosive, casing and the surrounding air. The fragment was hemispherically shaped with a length of 2.5cm and a diameter of 0.48cm. The casing was of a uniform thickness of 1.20cm encompassing a 3cm thick layer of explosive. A 0.04cm element size was used maintaining a 1:1 aspect ratio. The aluminium fragment was modelled using the Plastic Kinematic constitutive material model. The munitions RHA steel casing was modelled using the Johnson Cook constitutive material model. The explosive, Comp B, was modelled using the High Explosive Burn Elastic Plastic Hydrodynamic constitutive material model. The release of energy from the explosive was governed by the Ignition and Growth of Reaction in the High Explosive equation of state (IGRHE-EOS).

### 2.2 Simulation Configurations

Three configurations were simulated as listed in Table 1. They were based on an increase in fragment velocity to determine the critical velocity which would cause detonation of the explosive. The fragment impact orientation was normal to the surface along the center of the casing surface for all three cases.

Table 1: Numerical Configurations.

Case Number	Cover Thickness T, [mm]	Diameter of Fragment D, [mm]	T/D	Velocity [km/s]
Case A	1.2	4.8	0.25	1.00
Case B	1.2	4.8	0.25	2.00
Case C	1.2	4.8	0.25	3.35

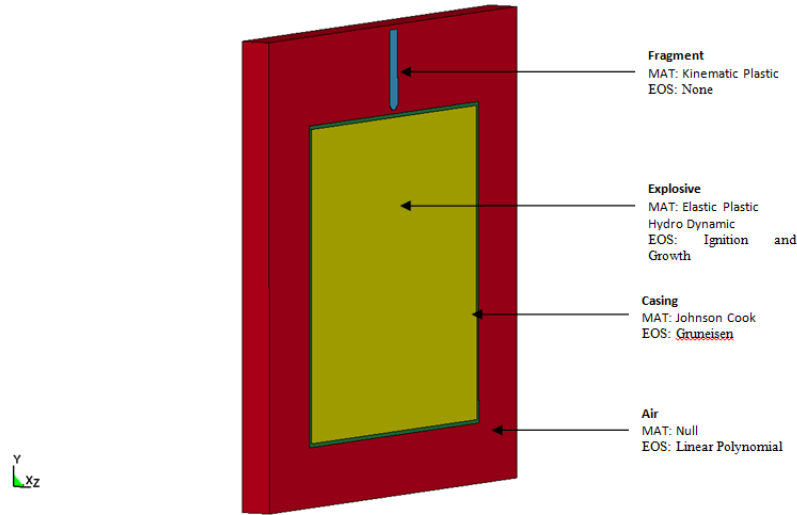


Figure 1: Finite Element Model.

### 2.3 Major Aspect of the Finite Element Model

LS-DYNA currently contains more than two hundred and thirty-nine constitutive models to cover a wide range of material behaviour. The constitutive models include those for which three variables are required to model a material and those which contain twenty six variables to model a material. The choice of which constitutive model to use is largely based the number of parameter values which are available and the degree of accuracy which is needed in the results. The material definition used in the simulation efforts are described below:

- 1) Elastic Plastic Hydrodynamic Constitutive Material Model: Composition B
- 2) Ignition and Growth in High Explosive Equation of State: Composition B
- 3) Johnson Cook Constitutive Material Model: RHA Steel
- 4) Mei-Gruneisen Equation of State: RHA Steel
- 5) Plastic Kinematic: Aluminum Fragment

#### 2.3.1 Elastic Plastic Hydrodynamic Constitutive Model Material (Composition B)

The explosive was simulated using the Elastic Plastic Hydrodynamic constitutive material model. This is the recommended material model to use when employing the IGIHE-EOS in LS DYNA. The material properties for Composition B are listed in Table 2 [7].

Table 2: Material Properties of Explosive (Composition B).

Parameter	Units	Composition B
Density ( $\rho$ )	[kg/m]	1713
Shear Modulus (G)	[GPa]	35.4
Yield Stress ( $\sigma_{yield}$ )	[GPa]	$0.2 \times 10^{-1}$

#### 2.3.2 Ignition and Growth of Reaction in High Explosive Equation of State

IGRHE – EOS was used to calculate the shock initiation or failure to initiate of solid high explosives. This EOS was based on model by Lee and Tarver [8] which showed that shock initiation of heterogeneous solid explosive should be modeled as at least a three step process. The first step was the formation of hot spots created by various mechanisms (compression,

viscous heating) during shock compression and the subsequent ignition (or failure to ignite due to heat conduction losses) of these heated regions. The second step in the process was assumed to be a relatively slow growth of reaction of the isolated hot spots. The third step in the shock initiation process was a rapid completion of the reaction as the reacting hot spots began to coalesce. This model is captured in equation (1), where the first term represents the ignition, the second term represents the grown and the third term represents the completion.

$$\frac{\partial F}{\partial t} = I(1 - F)^b \left( \frac{\rho}{\rho_0} - 1 - \alpha \right)^x + G_1(1 - F)^c P^d P^y + G_2(1 - F)^e P^f P^z \quad (1)$$

F is the mass fraction of explosive (F=0 implies no reaction, F=1 implies complete reaction), t is time,  $\rho_0$  is initial density,  $\rho$  is current density, P is pressure and I, G<sub>1</sub>, G<sub>2</sub>, a, b, c, d, e, f, x, y and z are material constants. Upper threshold limits F<sub>mixg</sub>, F<sub>mxGr</sub> and F<sub>mnGr</sub> are set to limit the contributions of the three terms respectively to a maximum reacted fraction F<sub>mixg</sub> for the first term, a maximum fraction F<sub>mxGr</sub> for the second term and a minimum fraction F<sub>mnGr</sub> for the last term. These limits are material dependant. The unreacted material properties for Comp. B are listed in Table 3 and the reaction parameters associated with equation (1) are listed in Table 4. Values for the unreacted and reaction products were referenced from [9].

Table 3: Unreacted Values for the IGRHE EOS (Comp. B)    Table 4: Reacted Values for the IGRHE EOS (Comp. B)

Parameter	Units	Values (Comp. B)	Parameter	Units	Values (Comp. B)
A	[GPa]	524.2	I	[s <sup>-1</sup> ]	4.00
B	[GPa]	7.678	a	[-]	3.67×10 <sup>-2</sup>
R <sub>1</sub>	[-]	778.1	b	[-]	6.67×10 <sup>-1</sup>
R <sub>2</sub>	[-]	-5.944×10 <sup>-2</sup>	c	[-]	6.67×10 <sup>-1</sup>
R <sub>3</sub>	[-]	2.46×10 <sup>-6</sup>	d	[-]	3.33×10 <sup>-1</sup>
R <sub>5</sub>	[-]	14.1	e	[-]	6.67×10 <sup>-1</sup>
R <sub>6</sub>	[-]	1.41	g	[-]	1.0
XP <sub>1</sub>	[-]	4.2	x	[-]	7.0
XP <sub>2</sub>	[-]	11	y	[-]	2.0
C <sub>vr</sub>	[Mbar K <sup>-1</sup> ]	2.487×10 <sup>-5</sup>	z	[-]	3.0
C <sub>vp</sub>	[Mbar K <sup>-1</sup> ]	1.0×10 <sup>-5</sup>	G <sub>1</sub>	[Mbar <sup>-2</sup> μs <sup>-1</sup> ]	140
T <sub>0</sub>	[K]	298	G <sub>2</sub>	[Mbar <sup>-2</sup> μs <sup>-1</sup> ]	1000
Shear Modulus (G)	[GPa]	380	F <sub>MXIG</sub>	[-]	2.2×10 <sup>-2</sup>
			F <sub>MXGr</sub>	[-]	7.0×10 <sup>-1</sup>
			F <sub>MNGr</sub>	[-]	0.0

2.3.3 Johnson Cook Constitutive Material Model (RHA-Steel)

The encasing structure was made from Rolled Homogenous Armour (RHA) steel. The face of the steel was hardened by heat-treatment of rolling and forging during the manufacturing process. This removes any imperfections which could reduce the strength of the steel. Rolling also elongates the grain structure in the steel to form long lines, which enables the stress under which the steel was placed to flow throughout the metal and not be concentrated in one area. The result is an enhanced ballistic performance of the steel attributed to higher level of hardness and ductility. RHA steel is largely used in military applications to manufacture armoured vehicles. The Johnson Cook (JC) constitutive material model was used to model the RHA steel with parameters taken from [10] and listed in Table 5. The JC constitutive material model is an empirical model which defines yield stress according to equation (2). Where A, B, C, n and M are material constants,  $\epsilon^p$  is the effective plastic strain and  $T^{*m}$  is the homologous temperature.

$$\sigma_y = (A + B\epsilon^p)^n (1 + C \ln \epsilon^p) (1 - T^{*m}) \quad (2)$$

Table 5: Parameters Johnson-Cook Material Model of RHA Steel.

Parameter	Units	RHA - Steel
Density ( $\rho$ )	[kg/m <sup>3</sup> ]	7850
Modulus (G)	[GPa]	77.5×10
Young's Modulus	[GPa]	200
Poisson Ratio	[-]	3.3×10 <sup>-1</sup>
Yield Stress (A)	[GPa]	4.90×10 <sup>-1</sup>
B	[GPa]	3.83×10 <sup>-1</sup>
N	[-]	4.5×10 <sup>-1</sup>
C	[-]	1.14×10 <sup>-2</sup>
M	[-]	9.4×10 <sup>-1</sup>
Melting Temperature (TM)	[K]	1800
Room Temperature	[K]	293
Specific Heat (CP)	[J/Kg-K]	4.77×10 <sup>-6</sup>
D <sub>1</sub> – D <sub>5</sub>	[-]	0.0
DTF	[-]	0.0
EPSO	[s <sup>-1</sup> ]	1×10 <sup>-6</sup>

2.3.4 Mei-Gruneisen Equation of State (EOS)

The Mie-Gruneisen EOS is a relation between the pressure and the volume of a solid at a given temperature. It is often used to determine the pressure in a shock-compressed solid. Equation 3 is used when the solid is in compression.

$$P = \frac{\rho C^2 \mu \left[ 1 + \left( 1 - \frac{T}{T_m} \right) \mu - \frac{\mu^2}{2} \right]}{\left[ 1 - (S_1 - 1) \mu - S_2 \frac{\mu^2}{\mu + 1} - S_3 \frac{\mu^3}{\mu + 1} \right]^2} + (\gamma + \alpha \mu) E \quad (3)$$

E is the internal energy of the RHA steel, C is the bulk speed of sound in RHA steel,  $\alpha$  is a first order correction to  $\gamma$ , the Gruneisen Gamma and is approximated as  $\gamma = \frac{\rho_0 \gamma_0}{\rho}$ , where  $\rho_0$  and  $\gamma_0$  are the density and Gruneisen parameter at the reference state of zero Kelvin and  $\rho$  is the density of RHA steel at the interested time. S<sub>1</sub>, S<sub>2</sub>, S<sub>3</sub> and A are the coefficients defining the slope of the Hugoniot curve for steel and  $u = \frac{P}{\rho_0} - 1$ . The Mei-Gruneisen parameters for RHA steel are summarized in Table 6 [10].

Table 6: Values for the Mei-Gruneisen Parameters RHA Steel.

Parameter	Units	RHA - Steel
C	[km/s]	39.4
S1	[-]	1.578
S2	[-]	0.00
S3	[-]	0.00
Gruneisen Gamma ( $\gamma$ )	[-]	1.69
A	[-]	0.00
Internal Specific Energy (E <sub>0</sub> )	GPa	0.00
Relative Specific Volume (V <sub>0</sub> )	[-]	0.00

### 2.3.5 Arbitrary Lagrangian Eulerian Multi Material Group (ALEMMG)

Arbitrary Lagrangian Eulerian formulation combines the Lagrangian and Eulerian methods of finite element analysis into a formulation which provides a much more robust method of element formulation in FEA. The advantage of this method over pure Lagrangian mesh formulation is its capability of dealing with large deformation, because the Lagrangian mesh is remapped back to its original position, elements remain uniform and deformation is captured with flow of material into the surrounding mesh.

ALE requires a domain mesh, which is modeled as a low density fluid for the material to flow through, typically the domain mesh is air or a vacuum. In this case the domain mesh was modeled as air. LS-DYNA uses ALEMMG to model the ALE formulation when more than two ALE parts interact. This allows for elements within the simulation to contain more than one part. Annex C gives the parameters which were used in LS-DYNA to define the ALEMMG keycard.

## 3. Results

The impact events were analyzed for a period of 30 $\mu$ s which was chosen to be sufficiently long to simulate the relevant events of this impact. The dynamic responses of the components were recorded at 0.05 $\mu$ s equal time steps. A summary of the three simulation cases along with their results is given in Table 7. Detailed discussion of the results is presented in the next section.

Table 7: Simulation Cases.

Simulation	Velocity [km/s]	End Time [ $\mu$ s]	Detonation	Detonation Cause
Case A	1.0	30.0	No	-
Case B	2.0	30.0	Yes	Hot Spots
Case C	3.35	30.0	Yes	Impact to Detonation

### 3.1 Discussion

The hemispherically aluminium fragment traveling at 1km/s impacting on the munitions generated 6.29GPa on the top surface of the casing as shown in Figure 2a (beginning on page 9). However, this pressure was reduced to 0.96GPa after it traversed the RHA steel casing (Figure 2b). The drop in pressure strength across the casing can be understood by using the one-dimensional formula (4) provided by [11] which gives an approximation for the pressure drop across the RHA steel interface.

$$\frac{P_T}{P_I} = \frac{2K_2}{K_2 + K_1} \quad (4)$$

$P_T$  is the transmitted pressure and  $P_I$  is the incident pressure.  $K$  is known as the shock impedance, defined as  $K = \rho \times U$ , where  $\rho$  is the density of the material before shock compression and  $U$  is the velocity of the shock wave in the material. Equation 4 gives the transmitted shockwave a magnitude of 1.5GPa. The discrepancy between the two numbers can be accounted for in the fact the above equation is a one dimensional approximation of the transmitted pressure and does not take into account three dimensional effects. The overall pressure drop can equally be understood by considering the fact that the shock (compressive stress) wave travelling downward encounters the front cover/explosive interface beyond which the shock impedance  $K$  of the medium is lowered. In such a case, the reflected pressure from the interface has a tensile component resulting in the pressure drop, since particle velocity is accelerated as the wave trespasses the interface.

In case B the impact generated a shock pressure of 15.9GPa on the top surface centered at the location of impact as shown in Figure 3a. This pressure however was reduced to 3.4GPa after it traversed the RHA steel casing by the same mechanism as discussed above. The initial pressure of 3.4GPa applied to the explosive is not enough to cause detonation and the incident shockwave traverses into the explosive unabated. As the pressure wave travels through the explosive areas behind the initial wave experiences compression, at approximately 12.95 $\mu$ s hot spots can be seen developing in Figure 4a. These hot spots occur behind the initial shockwave and are localized area of detonation due to that particular area being adiabatically compressed. In these small areas, the release of chemical energy is greater than the dissipated heat loss and the reaction grows forming a detonation wave shown in Figure 4b. From here on the large amount of energy being released by the detonation wave causes a runaway detonation and the pressure increases to 6.5GPa (Nearly doubling that of the initial pressure (3.4GPa) received by the explosive). The detonation wave eventually catches up with the incident shockwave and begins to lead it by impressing its pressure and velocity on the original wave. Full detonation can be seen with a maximum pressure of approximately 34.1GPa in Figure 4b. This phenomenon is known as run distance detonation and is defined as the distance the initial pressure wave travels into explosive before detonation occurs and is initial velocity dependent. In the case of 2km/s the run distance was 50mm.

Case C, represented the munitions casing after receiving the shock impulse from the aluminum fragment travelling at 3.35km/s. The pressure wave strength of 12.3GPa was enough to immediately cause detonation of the explosive, the so called impact to detonation phenomenon as shown in Figure 5a. The pressure in the detonation wave increased dramatically to 30.0GPa (see Figure 5b) at 2 $\mu$ s later, turning into a full self-sustaining detonation. This was unlike Case B, where the pressure wave had travelled some distance into the explosive before detonation.

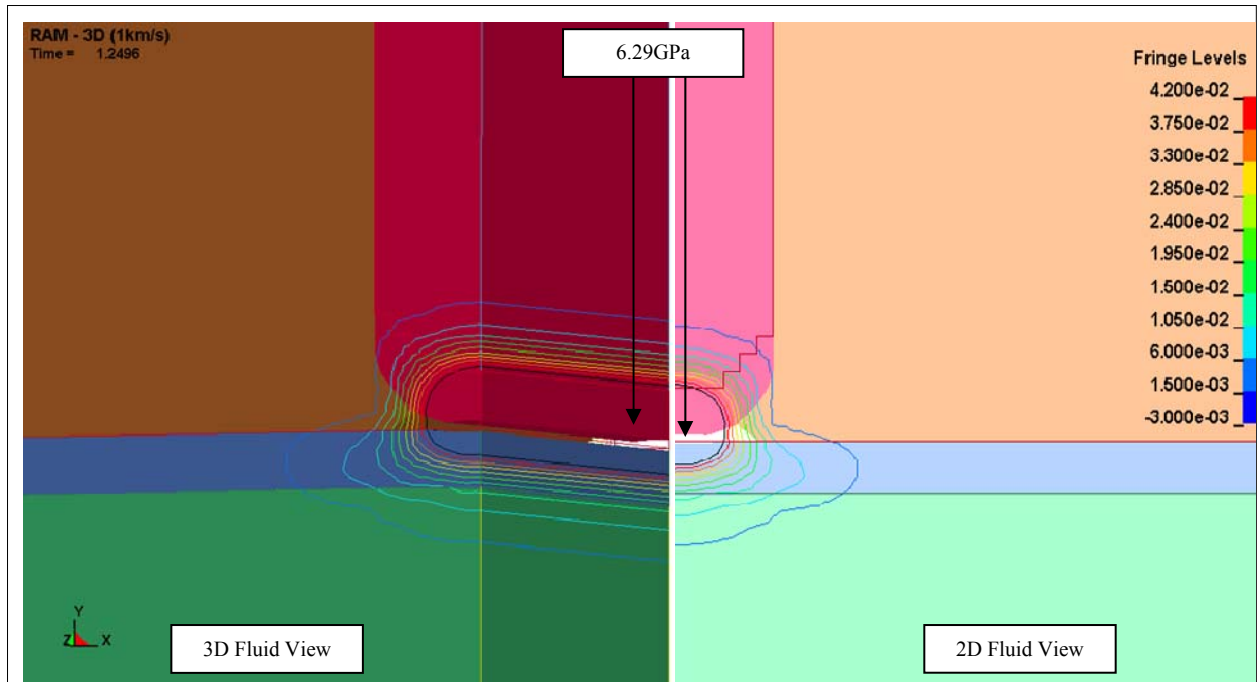
#### 4. CONCLUSION

Different types of shock-wave interactions triggering detonation in a RHA steel encapsulated explosive were numerically studied using the High Ignition and Growth Reaction in High Explosive equation of state model. The computational study was conducted using the Arbitrary Lagrangian Eulerian finite element model to analyze the relevant component of the simulation. The model provided data on the threshold detonation velocity (critical velocity), the resulting shockwave propagation and pressure profile.

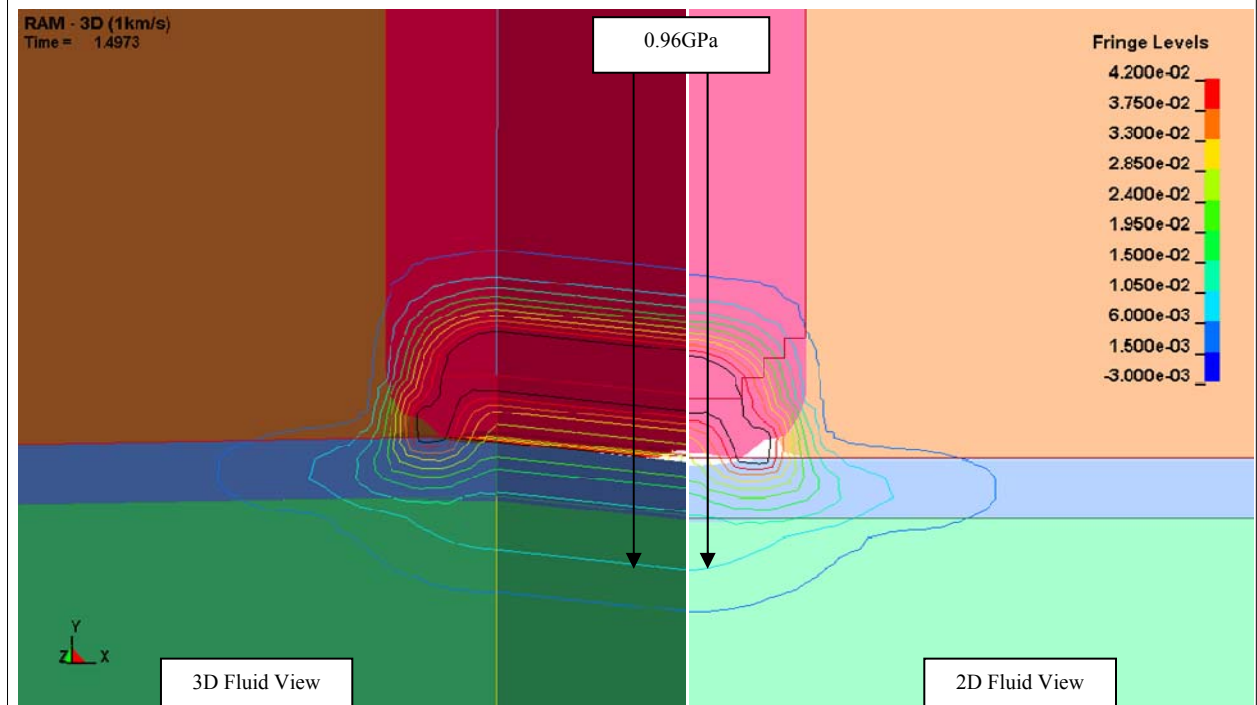
The following conclusions were drawn from the parametric study of a hemispherical aluminium fragment at impact velocity. After the formation of an impact of the fragment on the front cover plate, a shockwave originates at the location of impact and is transmitted through to the explosive at a reduced magnitude due to shock impedance of the RHA steel. The shock front transmitted into the explosive may cause detonation in a number of ways depending on its magnitude. Low velocity impact may not generate a shockwave strong enough to cause detonation of the explosive or initiation may come from the result of the superposition of the incident shockwave with high pressure zones in the explosive. Hot Spots start to form as the pressure rises in these localized areas and, full detonation occurs when the Hot Spots begin to coalesce and/or a second high pressure zone merges with the Hot Spots. For impacts at the intermediate velocity the presence of the back plate increases the explosive sensitivity to detonation due to the fact the compression of the incident shockwave may generate a pressure wave high enough to cause detonation. High velocity impact may cause detonation of the explosive immediately after the shockwave has been transmitted through the cover plate interface and interact with the explosive. The formation of the first Hot Spot can be seen forming however, this only lasts for a few microseconds as the fragment continues to increase the pressure in these localized area. The full detonation wave starts to spread out eventually catching up to the initial shockwave, turning the explosive material into detonation products.

#### References

- [1] Gurney, R., *"The Initial Velocities of Fragments from Bombs, Shells and Grenades"* BRL Report No. 405. Aberdeen Proving Ground, Maryland, 1943.
- [2] Held, M. *"Reaction Thresholds in Unconfined and confined Charges by Shock Load"*, Projectile, Propellants, Explosives, Pyrotechnics, Vol. 25, pp. 107-11, 2000.
- [3] Griffiths N., Laidler R.M., Spooner S.T., *"Some Aspects of the Shock Initiation of Condensed Explosives"* Combust Flame Vol. 7, pp 347-352, 1963.
- [4] Roslund L.A., Watt J.M., Coleburn N.L., *"Initiation of Warhead Explosives by the Impact of Controlled Fragments in Normal Impact"*. Report No. NOLTR 73-124. Naval Ordnance Laboratory, White Oak, MA, USA, 1975.
- [5] Lawrence, W., *"A Computational Study to Determine the Critical Velocity Required to Initiate Explosively Loaded Munitions"*, High Performance Computing Modernization Program Users Conference, 18-21 June 2001.
- [6] Hallquist, J.O., *"LS-DYNA Keyword User's Manual Version 971"*, Livermore Software Technology Corporation, Livermore, CA, 2013.
- [7] Murphy, M.J., Lee, E.L., Weston, A.M., Williams, A.E., *"Modeling Shock Initiation in Composition B"* Detonation Symposium, Boston Mass, July 12 – 16, 1993.
- [8] Lee, E. L., Tarver, C. M. *"Phenomenological Model of Shock Initiation in Heterogeneous Explosives"* Physics of Fluid, Vol. 23 pp 2362. 1980.
- [9] Urtiew, P.A. Vandersall, K.S., Taver C. M., Garcia, F. Forbes, J.W. *"Shock Initiation Experiments and Modeling of Composition B and C-4"* 13 International Detonation Symposium Nofold, VA, 2006.
- [10] Jutras, M. *"Improvement of the Characterisation Method of the Johnson-Cook model"* faculte des sciences et de genie universite Laval Quebec, 2008.
- [11] Shin, H., Lee W., *"A Numerical Study on the Detonation Behaviour of Double Reactive Cassettes by Impacts of Projectiles with Different Nose Shapes"*, International Journal of Impact Engineering, Vol. 28, 2003.



a) Maximum pressure experience by casing



b) Maximum pressure experienced by the explosive

Figure 2: Maximum Pressure on Casing and explosive (Case A)

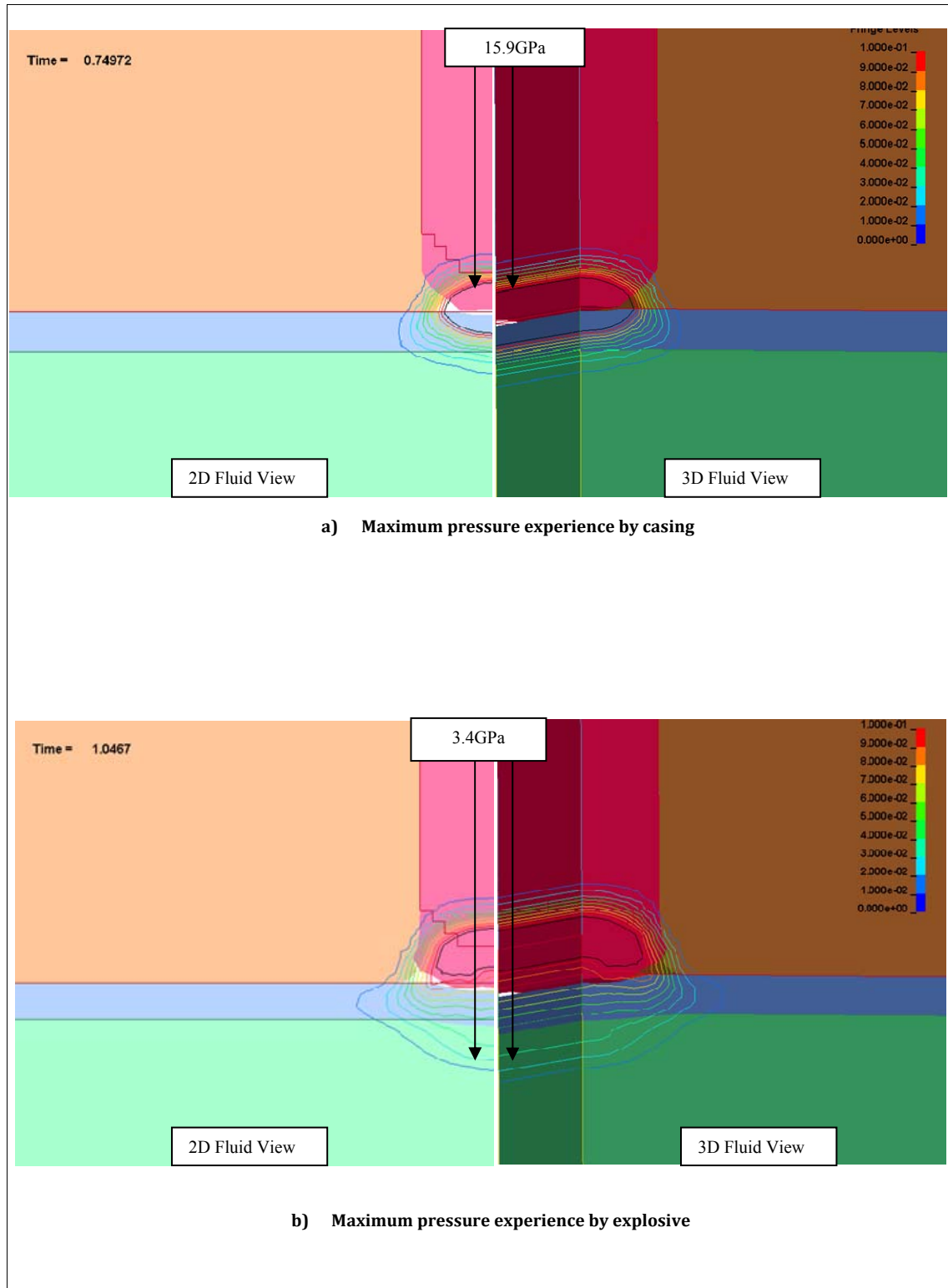
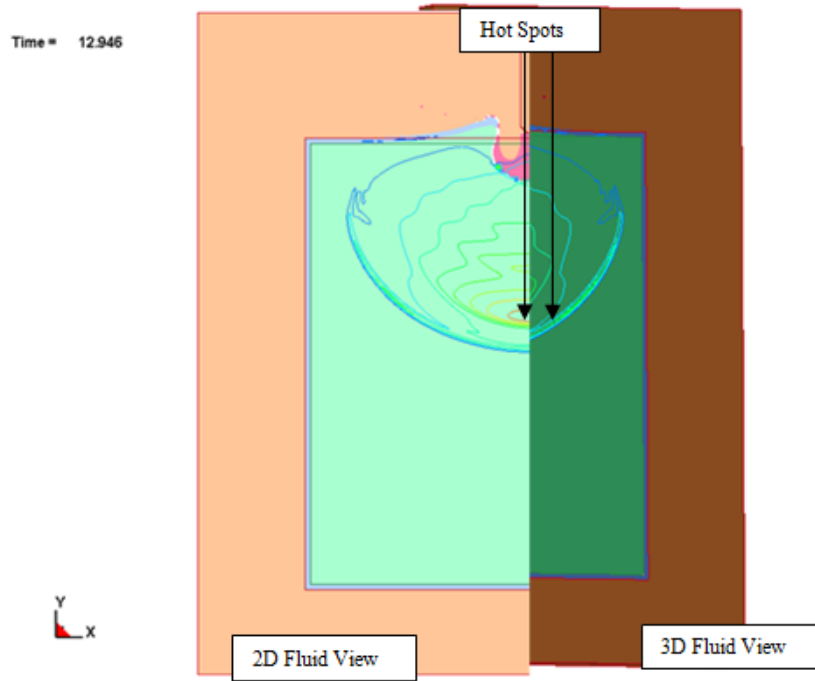
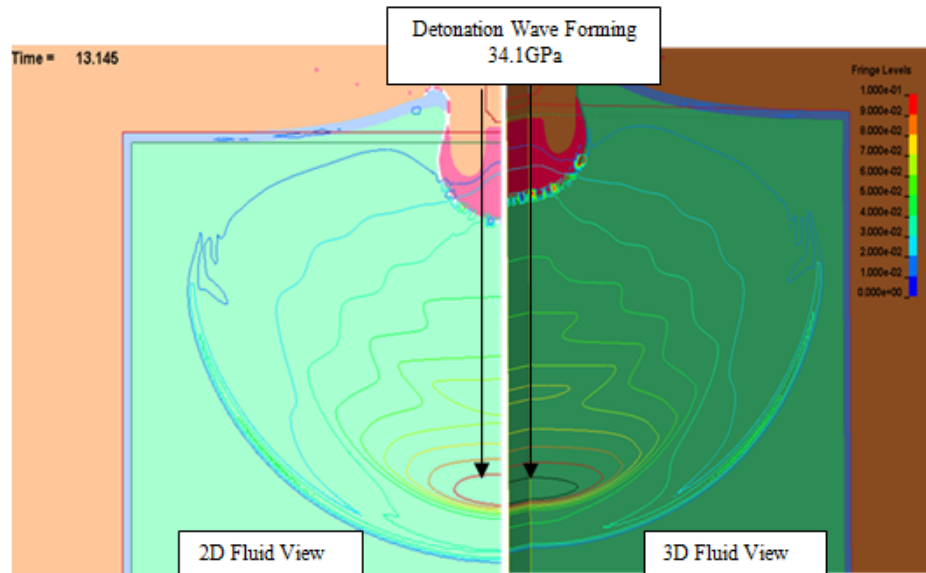


Figure 3: Location of Maximum Pressure at Impact Pressure Contour (Case B)



a) Hot Spots developing in explosive



b) Detonation occurring due to hot spots growing

Figure 4: Development of Hot Spots (Case B)

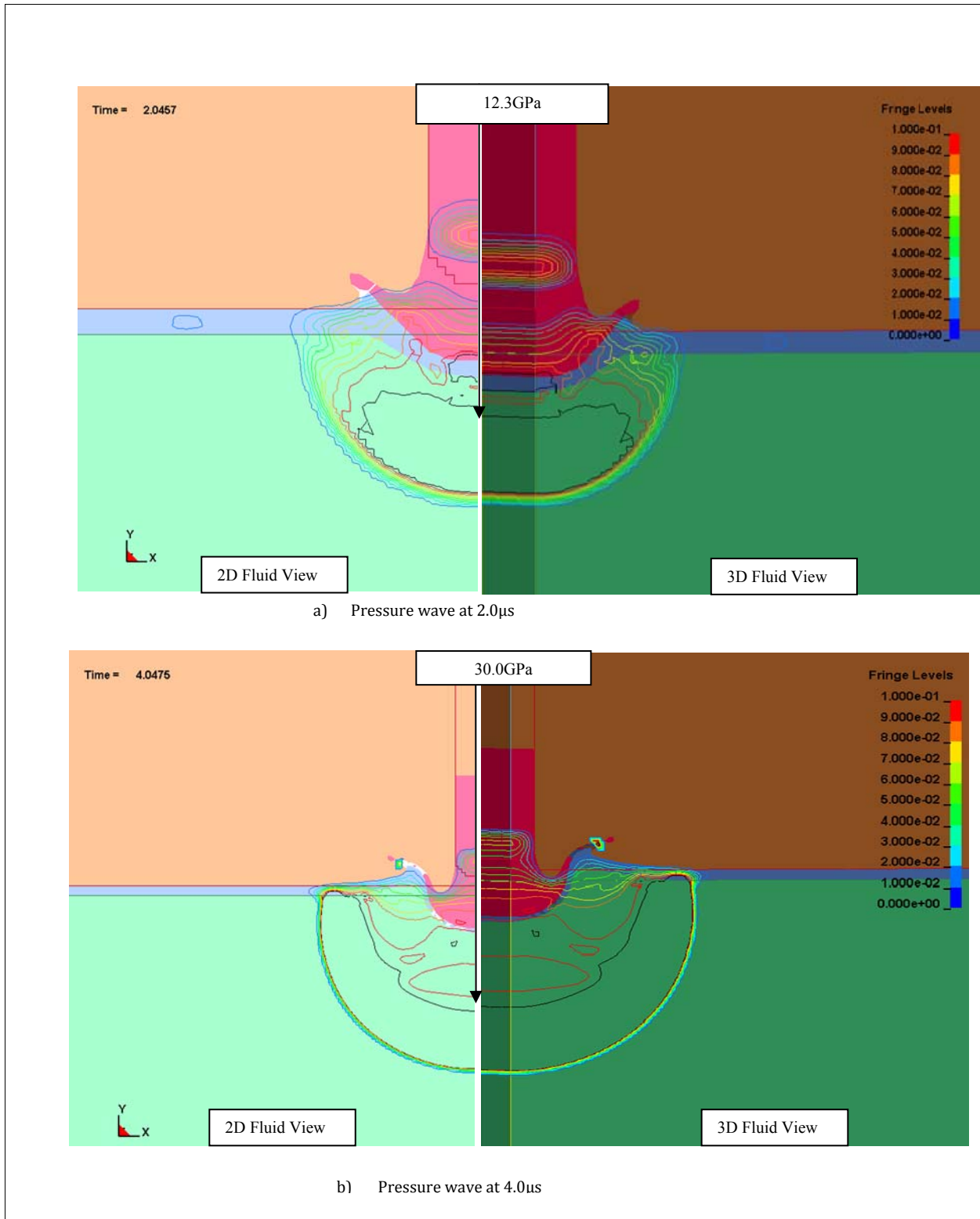


Figure 5: Full Detonation of Explosive (Case C)